

TTT-KD: Test-Time Training for 3D Semantic Segmentation through Knowledge Distillation from Foundation Models

Lisa Weijler¹ M. Jehanzeb Mirza^{2,3} Leon Sick⁴ Can Ekkazan⁵
Pedro Hermosilla¹

¹TU Wien, Austria. ²ICG, TU Graz, Austria. ³CDL-EML. ⁴Ulm University
⁵Yildiz Technical University

Abstract. Test-Time Training (TTT) proposes to adapt a pre-trained network to changing data distributions on-the-fly. In this work, we propose the first TTT method for 3D semantic segmentation, **TTT-KD**, which models Knowledge Distillation (KD) from foundation models (*e.g.* DINOv2) as a self-supervised objective for adaptation to distribution shifts at test-time. Given access to paired image-pointcloud (2D-3D) data, we first optimize a 3D segmentation backbone for the main task of semantic segmentation using the pointclouds and the task of 2D \rightarrow 3D KD by using an off-the-shelf 2D pre-trained foundation model. At test-time, our TTT-KD updates the 3D segmentation backbone for each test sample, by using the self-supervised task of knowledge distillation, before performing the final prediction. Extensive evaluations on multiple indoor and outdoor 3D segmentation benchmarks show the utility of TTT-KD, as it improves performance for both in-distribution (ID) and out-of-distribution (OOD) test datasets. We achieve a gain of up to 13% mIoU (7% on average) when the train and test distributions are similar and up to 45% (20% on average) when adapting to OOD test samples.

1 Introduction

3D semantic segmentation represents a fundamental benchmark for neural networks that process pointclouds [7, 18, 53, 58]. In this task, the model’s primary objective is to predict the semantic label of each point in the scene. Successful execution of this task requires a profound comprehension of scene objects and their precise spatial localization. Despite the recent success obtained by different models for the task of 3D semantic segmentation, the generalization of these models on different data sets still remains an open problem. This generalization gap can be provoked due to a variety of reasons: sensors used during acquisition, reconstruction algorithms used to obtain the pointcloud, inherent noise on the point coordinates, colors, and normals, or even the different scene compositions.

One way to bridge the domain gap is to label the pointcloud sequences from different datasets and train the network in a supervised manner on this data [56].

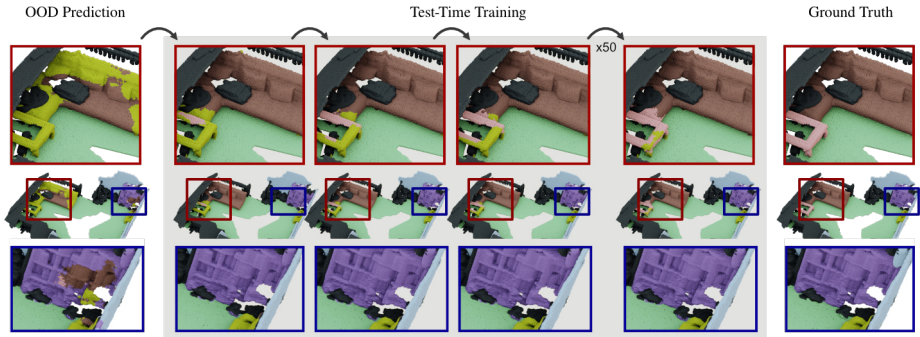


Fig. 1: TTT-KD. We propose the first test-time training method for 3D semantic segmentation which adapts to distribution shifts at test time. As shown in the illustration above, our method is able to adapt to Out-of-Distribution (OOD) scenes (SCANNET) where the model was not trained on (S3DIS). Iteratively, via knowledge distillation from 2D foundation models, our algorithm adjusts the weights of the network, progressively improving prediction with each step (**top**). Moreover, our approach is able to significantly improve the predictions with even a single step while maintaining the quality of those without degradation over multiple steps (**bottom**).

However, labeling can incur huge monetary costs and manual effort. To avoid these challenges several works suggested to adapt the network in an unsupervised manner to the OOD data. A popular paradigm is Unsupervised Domain Adaptation (UDA), where the network is trained jointly on the labeled source domain and unlabeled target domain, with the goal of learning an invariant feature representation for both domains. Many works [4, 42–45, 63], have proposed UDA approaches for 3D semantic segmentation for outdoor pointclouds, but countering domain shifts for indoor scenes is relatively less studied. Moreover, in real-world scenarios, there could rarely be situations where the target domain is known in advance, rendering these methods unsuitable.

To forego the need for access to the target domain data, Test-Time Adaptation (TTA) algorithms [25, 48, 54] instead propose to adapt the network weights at test-time, more generally with some posthoc regularization. For effective adaptation, these works usually require constrained optimization of the network parameters, for example, only updating the affine parameters of the normalization layers. However, this could be insufficient to adapt to severe domain shifts. Moreover, these methods also rely on larger batch sizes for adaptation, making their applicability to large indoor 3D scenes challenging.

Sharing the philosophy with TTA of adapting the network weights at test-time but differing in its application and methodology, TTT proposes to first train a network jointly for the main (downstream) task and a self-supervised auxiliary objective. At test-time, given a (single) pointcloud sample, TTT adapts the network weights *independently* for each pointcloud sample by using the self-supervised objective, and then performs inference with the adapted network weights. Recently, MATE [31] proposes to use Masked Auto Encoding

(MAE) [38] task as a self-supervised objective for adaptation to OOD pointclouds at test-time, for the task of pointcloud classification. However, its architecture makes it unsuitable for application to dense prediction tasks, such as 3D semantic segmentation, and it was only tested on synthetic domain shifts.

In this work, we propose the first TTT algorithm for the task of 3D semantic segmentation, TTT-KD, which models $2D \rightarrow 3D$ KD from foundation models as a self-supervised objective. During training, our method receives a 3D pointcloud as input and a set of 2D images of the same scene with point-pixel correspondences. A 3D backbone processes the 3D pointcloud generating a set of 3D per-point features. These 3D features are then used to predict the semantic label of the points and also to perform $2D \rightarrow 3D$ KD from a 2D foundation model, DINOv2 [37] in most of our experiments. At test-time, given a test pointcloud with its corresponding images, we adapt the network’s weights by taking several gradient descent steps on the self-supervised task of KD. Since the 3D backbone has learned a joint feature space for the main segmentation task and the self-supervised KD task, improving predictions on the KD task leads to large improvements in the semantic segmentation task. Our algorithm does not make any assumption of the target domain and, therefore, it is able to adapt to it by processing individual scenes at a time. Our extensive evaluation shows that our algorithm not only leads to large improvements for OOD datasets (see Fig. 1), up to 17 in mean Intersection over Union (mIoU), but also provides significant improvements on in-distribution datasets, up to 8.5 in mIoU.

2 Related Work

Our TTT-KD is related to works which study Unsupervised Domain Adaptation (UDA), Test-Time Adaptation (TTA), and more closely to works which propose methodologies for Test-Time Training (TTT).

Unsupervised Domain Adaptation. UDA aims to train a network in order to bridge the gap between the source and target domains while having access to labeled data from the source domain and unlabeled data from the target domain. For the task of pointcloud classification, PointDAN [40] proposes to learn domain invariant features between the source and target domain with the help of adversarial feature alignment [13]. Liang *et al.* [24] propose to learn an invariant feature space for the source and target domain by using self-supervision. More specifically, they propose to predict the masked local structures by estimating cardinality, position and normals for the points in the source and target domains, while Shen *et al.* [47] propose to use implicit functions coupled with pseudo-labeling for UDA. For 3D object detection, some approaches [30, 55] rely on statistical normalization of the anchor boxes in the source and target domain for UDA. Lehner and Gasperini *et al.* [23] propose to use adversarial augmentations, while pseudo-labeling is employed by [11, 29, 44, 61]. The task of 3D semantic segmentation has also been studied extensively in the context of UDA. Yi *et al.* [63] propose to synthesize canonical domain points, making the sparse

pointcloud dense, before performing segmentation. Saltori *et al.* [42] propose a pseudo-labeling approach by mixing the source and target domains. xMUDA [21] proposes a multi-modal (two-stream) learning approach between 3D and 2D networks, they perform UDA by minimizing the discrepancy between the feature space of the two streams and self-training through pseudo-labeling. Some other approaches also rely on a multi-modal setup and achieve UDA by increasing the number of samples used from 2D features by increasing the 3D to 2D correspondences [39], employing contrastive learning [60] or leveraging SAM [22] for obtaining reliable dense 2D annotations [4]. Although UDA offers an efficient solution for adaptation to distribution shifts, still it requires advanced knowledge about the target distribution and requires access to the unlabeled data as well. However, in real-world scenarios, it is often the case that such luxury is not affordable. Distribution shifts can occur *on-the-fly* and can be unpredictable. Thus, a more practicable solution is to adapt the network weights whenever changing data distributions are encountered, which is put forward by TTT.

Test-Time Adaptation. TTA does not alter the training procedure of the network but instead proposes post hoc regularization for adaptation to distribution shifts at test-time. For the image domain, some approaches rely on statistical correction to adapt the network at test-time, generally by adapting the means and variance estimates (of the Batch Normalization layer [19]) to the OOD test data [26, 32]. TENT [52] proposes to adapt to distribution shifts at test-time by minimizing the Shannon Entropy [46] of predictions and adapts only the scale and shift parameters of the normalization layers in the network. The problem of TENT [52] to require larger batch sizes is solved by MEMO [64], which augments a single sample multiple times and minimizes the marginal output distribution over the augmented samples. Niu *et al.* [36] proposes a sharpness aware entropy minimization method for adaptation to distribution shifts in the wild. One group of TTA methods also rely on self-training. T3A [20] casts TTA as a prototype learning problem and replaces a classifier learned on the source dataset with pseudo-prototypes generated on-the-fly for the test batch. AdaContrast [6] uses contrastive learning with a momentum encoder to adapt to distribution shift on-the-fly. MM-TTA [48] uses 2D-3D multi-modal training for test-time adaptation but only adapts batch normalization affine parameters with a pseudo-labeling strategy. Liang *et al.* [25] also relies on pseudo-labeling and entropy minimization of individual predictions but also encourages maximizing the entropy over predicted classes over the entire dataset. CoTTA [54] also relies on pseudo-labeling and proposes continual test-time adaptation, where they learn different distribution shifts at test-time in a continual manner. Similarly, other continual TTA methods include [10, 35]. Another group of methods also relies on consistency of predictions [3], or statistics between the train and test data distributions [27, 33]. We port AdaContrast [6], DUA [32] and TENT [52] to the task of 3D semantic segmentation and, together with MM-TTA [48], choose them as representative methods for TTA. Empirically, our TTT-KD outperforms these methods comprehensively on all the benchmarks we test on.

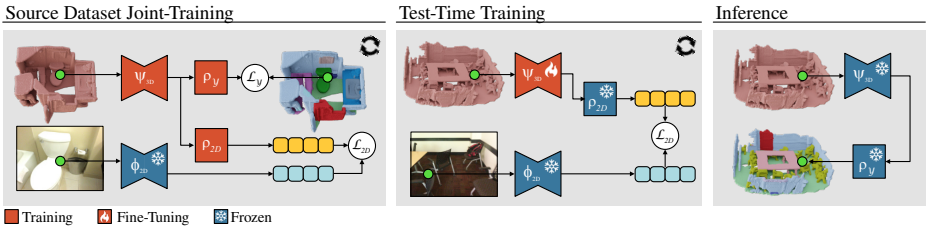


Fig. 2: Given paired image-pointcloud data of a 3D scene, TTT-KD, during **joint-training**, optimizes the parameters of a point or voxel-based 3D backbone, ψ_{3D} , followed by two projectors, ρ_Y and ρ_{2D} . While ρ_Y predicts the semantic label of each point, ρ_{2D} is used for knowledge distillation from a frozen 2D foundation model, ϕ_{2D} . During **test-time training**, for each test scene, we perform several optimization steps on the self-supervised task of knowledge distillation to fine-tune the parameters of the 3D backbone. Lastly, during **inference**, we freeze all parameters of the model to perform the final prediction. By improving on the knowledge distillation task during TTT, the model adapts to out-of-distribution 3D scenes different from the source data the model was initially trained on.

Test-Time Training. TTT first proposes to train the network jointly for the main downstream task (*e.g.*, 3D Semantic Segmentation in our case) and a self-supervised objective. At test-time, it adapts the network weights, for a single OOD sample as it is encountered, by using the self-supervised objective – usually by taking multiple gradient steps for each sample. TTT methods are usually strictly *inductive* in nature, *i.e.*, they adapt the network weights on a single sample only, whereas, TTA methods do not adhere to this restriction. For the image domain, there are two TTT works that differ *w.r.t* the self-supervised objectives they employ for adaptation. The first TTT [50] method (which popularized the name) employs rotation prediction [15] as its self-supervised task. Unfortunately, this approach is difficult to adapt to 3D semantic segmentation, since 3D scenes do not have a canonical orientation, and training with random $SO(3)$ rotations usually leads to a degradation in the resulting performance. The second TTT approach, TTT-MAE [12], uses the task of image reconstruction through masked auto-encoders (MAE) [16]. MATE [31] proposes a TTT method, which also employs the MAE objective (PointMAE [38] for pointclouds) for adapting to distribution shifts in pointclouds. MATE shows impressive performance for the task of pointcloud classification but uses an architecture that is unsuitable for 3D semantic segmentation, which is the focus of our work.

In this paper, we propose a TTT method which models (2D \rightarrow 3D) Knowledge Distillation from foundation models (*e.g.*, DINOv2 [37]) as a self-supervised objective for adaptation to distribution shifts at test-time, for the task of 3D semantic segmentation. Similar to other TTT works, our TTT-KD is also strictly inductive in nature and adapts on a single pointcloud sample by performing multiple gradient steps for effective adaptation.

3 Methods

Our algorithm jointly trains a 3D model on the semantic segmentation task and 2D \rightarrow 3D KD as a secondary self-supervised task. In order to be robust to domain shifts, for each scene during testing, we perform a few steps of gradient descent on the KD task before we freeze the model to perform the final prediction on the segmentation task. In this section, we explain the three phases of our method: *Joint Training*, *Test-Time Training*, and *Inference* (see Fig. 2).

3.1 Input

Our method assumes as input sets of the form $(\mathcal{X}, \mathcal{F}, \mathcal{Y}, \mathcal{I}, \mathcal{U})$, where $\mathcal{X} \in \mathbb{R}^{N \times 3}$ are the spatial coordinates of the N points representing the scene, $\mathcal{F} \in \mathbb{R}^{N \times F}$ are the features associated with each point, $\mathcal{Y} \in \{0, 1\}^{N \times C}$ are per-point semantic labels, $\mathcal{I} \in \mathbb{R}^{I \times W \times H \times 3}$ are a set of I images of the same scene, and $\mathcal{U} \in \mathbb{R}^{I \times N \times 2}$ are the pixel coordinates of each pair of point in \mathcal{X} and image in \mathcal{I} . Note that not all points are projected on all images, and some points of the scene might not be projected on any image.

3.2 Joint Training

3D backbone. During training, we process each pointcloud \mathcal{X} with a 3D backbone ψ_{3D} to generate semantically relevant 3D features per-point, F^{3D} . Our method is agnostic to the backbone used and works, as we will show later, with voxel-based and point-based architectures.

2D foundation model. At the same time, we process all images of the 3D scene, \mathcal{I} , with a model ϕ_{2D} capable of generating semantically relevant 2D features, F^{2D} . This foundation model is pre-trained in a self-supervised manner on millions of images and remains fixed during the whole training procedure. As we will show in the ablation studies, our method is also agnostic to the foundation model used and can be used with any off-the-shelf foundation model.

Learning objective. Our learning objective is a multi-task objective where, from the 3D features F^{3D} , we aim to predict the semantic label of each point, $\hat{\mathcal{Y}}$, and the associated average 2D feature \hat{F}^{2D} over all the images. Therefore, our algorithm minimizes a combination of two losses:

$$\begin{aligned} \mathcal{L}_{\mathcal{Y}} &= \mathbb{E}_{x \sim \mathcal{X}} \left[- \sum_c^C \mathcal{Y}_{x,c} \log(\hat{\mathcal{Y}}_{x,c}) \right] \\ \mathcal{L}_{2D} &= \mathbb{E}_{x \sim \mathcal{X}, i \sim \mathcal{I}} \left[- \frac{\hat{F}_x^{2D}}{\|\hat{F}_x^{2D}\|} \cdot \frac{F_i^{2D}(\mathcal{U}_{x,i})}{\|F_i^{2D}(\mathcal{U}_{x,i})\|} \right] \end{aligned}$$

where $\mathcal{L}_{\mathcal{Y}}$ is the cross-entropy loss between the predicted labels $\hat{\mathcal{Y}}$ and the ground truth labels \mathcal{Y} , and \mathcal{L}_{2D} is the knowledge distillation loss defined as the expected

cosine similarity between the normalized per point features \hat{F}^{2D} and image features F^{2D} , sampled at the pixel position defined by the mapping \mathcal{U} . To estimate \mathcal{L}_Y during training, we compute the average cross-entropy loss of all the points within the batch. However, since estimating \mathcal{L}_{2D} is more expensive, we randomly sample points x and images i to fill a certain budget per batch.

Feature projection. In order to learn a common 3D feature space F^{3D} with these competing objectives without hampering the predictions on the main task, we transform the 3D features to \hat{Y} and \hat{F}^{2D} with two separate projectors, ρ_Y and ρ_{2D} respectively. In practice, these projectors are two simple Multi-layer Perceptron (MLP). During training, we optimize the parameters of the 3D backbone, ψ_{3D} , and the two projectors, ρ_Y and ρ_{2D} , whilst the parameters of the foundation model, ϕ_{2D} , remain fixed.

3.3 Test-Time Training

Contrary to the standard testing phase in other algorithms, in which the parameters of the model are frozen, our algorithm, for each OOD scene, slightly modifies the parameters of the model before performing the final prediction. In particular, we freeze the parameters of the projectors ρ_Y and ρ_{2D} , and fine-tune all parameters of ψ_{3D} while fixing the mean and standard deviation of the batch normalization layers. In particular, we perform several gradient descent steps minimizing the knowledge distillation loss, \mathcal{L}_{2D} , for which no labels are required. Since both projectors have learned to perform predictions from a common feature space, F_{3D} , and both projectors aim to predict semantically relevant information, modifying these features to improve \mathcal{L}_{2D} also improves the predictions on the primary segmentation task. Since we process single scenes, contrary to existing test-time adaptation approaches, we do not update the mean and standard deviation of the batch normalization layers. Therefore, we are not forced to synthetically increase the batch size with data augmentations, which might be prohibitive for large scenes composed of millions of points.

3.4 Inference

Once the test-time training phase has finished, we freeze all parameters of our model and perform the final prediction on the segmentation task. Following previous works [31, 50], we experiment with two variants of our method:

Offline (TTT-KD). In this setup, we perform several gradient descent steps for each test scene independently. Once the TTT phase has finished, we predict the per-point class for the current scene and then we discard the parameter updates before processing the next test scene.

Online (TTT-KD-O). In this setup, we only perform one optimization step for each test scene but we keep the parameter updates between consecutive scenes. Although this approach does not fully adapt to a single scene, it requires less computational resources while, as we will show later, achieving significant improvements over the baselines.

4 Results

In this section, we describe the experiments carried out to validate our methods. In particular, we tested our TTT-KD algorithm on two different 3D semantic segmentation setups: indoor and outdoor 3D semantic segmentation. While indoor 3D semantic segmentation provides an ideal setup for our algorithm, in which each pointcloud is paired with multiple 2D images, outdoor 3D semantic segmentation presents a more challenging setup in which only a single 2D image is paired with each pointcloud.

4.1 Indoor 3D Semantic Segmentation

In this section, first, we describe the datasets used to validate our TTT-KD, then explain our experimental setup, and lastly, we provide the results.

Datasets. In our experiments, we use three different datasets of real indoor 3D scenes, SCANNET [8], S3DIS [1], and MATTERPORT3D [5]. These datasets are composed of several 3D scans of rooms from different buildings for which the reconstructed 3D pointcloud and a set of 2D images per pointcloud are available. We follow the standard train, validation, and test splits of the datasets in our experiments. For each point in the 3D scan, 3D coordinates, $[x, y, z]$, its normal, $[n_x, n_y, n_z]$, and color, $[r, g, b]$, are used as input to the models.

Experimental setup. In this section, we describe the experimental setup used. Additional details are provided in the appendix.

Tasks. We focus on two types of evaluations for our TTT-KD: ID and OOD. For ID evaluation, we train a model on the train split of a dataset and perform TTT on the test split on the same dataset, while for OOD, TTT is performed on the test split of all other datasets in our evaluation setup. We report results by using the mIoU evaluation metric for semantic segmentation. For OOD evaluations, since different datasets differ on the semantic labels used, we evaluate only the classes in which both the train and test dataset share.

Models. Our experiments use two different 3D backbones: a voxel-based and a point-based architecture. As our voxel-based backbone, we choose the commonly used Minkowski34C [7]. The point-based backbone is taken from Hermosilla *et al.* [18] which is based on kernel point convolutions with Gaussian correlation functions. As our foundation model, we use DINOv2 [37], in particular, the ViT-L/14 model with an embedding size of 1024 features.

Testing. During training, we randomly rotate scenes along the up vector. Therefore, during testing, we accumulate the logits over 8 predictions of the same scene but rotated with different angles, covering 360 degrees. In the TTT phase, we use Stochastic Gradient Descent (SGD) without momentum and a large learning rate of 1, and perform 100 optimization steps for each rotated scene on the offline version of our algorithm, but only one for the online version.

Baselines. We train our models on the main segmentation task, *Source-Only*, and also using knowledge distillation as a secondary objective, *Joint-Train*. We compare their performance to the offline version of our algorithm, *TTT-KD*, and the online version, *TTT-KD-O*. Since, in the literature, there is no TTT method proposed for the task of 3D semantic segmentation, we port several works from the image domain. Specifically, we compare our method with *TENT* [52], *DUA* [32], and *AdaContrast* [6]. While *TENT* uses entropy minimization at test-time, *DUA* updates the mean and standard deviation of the batch normalization layers. *AdaContrast*, on the other hand, leverages contrastive learning and momentum encoder to adapt the parameters of the model during testing. Lastly, for OOD experiments, as an upper bound, we provide the performance of an oracle model that has been trained on the same dataset as the test set, *Oracle*.

Results. The main experimental results and comparisons with all other methods are provided in Tab. 1. In the following, we explain these results in detail.

Joint-Training. First, we compare the performance of a Source-Only model with our Joint-Train strategy. Our results in Tab. 1 show that for all datasets and both 3D backbones, joint training always provides an improvement over the Source-Only model. In some cases, this improvement is minor, such as in SCANNET or MATTERPORT3D with an improvement of 0.8 mIoU, but for other datasets the improvement is larger, as in S3DIS or in MATTERPORT3D \rightarrow SCANNET with an improvement of 2.2 and 3.6 mIoU respectively. We conjecture that the reason for the improvement is the KD task acts as an additional regularizer.

In-distribution. When testing on ID data, our algorithm provides significant improvements for all three datasets and all 3D backbones. Our algorithm presents an improvement of 2.9 and 3.7 for SCANNET, of 8.5 and 5.6 for S3DIS, and 3.5 and 2.7 for MATTERPORT3D. Moreover, although smaller, the online version of our algorithm, TTT-KD-O, also presents significant gains on all datasets.

Out-of-distribution. When we look at the performance of the Source-Only models when tested on OOD data, as expected, the performance drops significantly when compared with an Oracle model trained on ID data, with large drops in performance as in MATTERPORT3D \rightarrow SCANNET with 24.5 or in S3DIS \rightarrow SCANNET with 30.1. Our TTT-KD algorithm, on the other hand, is able to reduce this gap, increasing significantly the performance of all models and even obtaining better performance than the Oracle model as in the SCANNET \rightarrow MATTERPORT3D experiment. Again, our online version, TTT-KD-O, also provides significant improvements but is smaller than our offline version.

Table 1: Our method achieves large improvements not only on OOD data but also on ID setups, surpassing existing methods by a large margin. Moreover, these results show that our algorithm is backbone agnostic, achieving comparable results for a point-based backbone, PNE [18], and a voxel-based backbone, Mink [7].

Train	Method	Test					
		SCANNET		S3DIS		MATTERPORT3D	
		PNE [18]	Mink [7]	PNE [18]	Mink [7]	PNE [18]	Mink [7]
SCANNET	Oracle	–	–	75.7	77.4	53.9	52.3
	Source-Only	73.5	72.9	65.8	67.3	49.1	48.3
	Joint-Train	74.3 \uparrow 0.8	73.9 \uparrow 1.0	66.5 \uparrow 0.7	71.5 \uparrow 4.2	50.4 \uparrow 1.3	48.7 \uparrow 0.4
	TENT	71.1 \downarrow 2.4	68.8 \downarrow 4.1	46.8 \downarrow 19.0	70.5 \uparrow 3.2	47.1 \downarrow 2.0	44.1 \downarrow 4.2
	DUA	73.9 \uparrow 0.4	73.1 \uparrow 0.2	64.0 \downarrow 1.5	70.6 \uparrow 3.3	48.9 \downarrow 0.2	46.9 \downarrow 1.4
	AdaContrast	73.8 \uparrow 0.3	72.4 \downarrow 0.5	67.2 \uparrow 1.4	72.3 \uparrow 5.1	50.2 \uparrow 1.1	48.4 \uparrow 0.1
	TTT-KD-O	75.5 \uparrow 2.0	74.7 \uparrow 1.8	72.4 \uparrow 6.6	73.7 \uparrow 6.4	53.6 \uparrow 4.5	51.3 \uparrow 3.0
	TTT-KD	76.4 \uparrow 2.9	76.6 \uparrow 3.7	70.4 \uparrow 4.6	73.1 \uparrow 5.8	56.6 \uparrow 7.5	55.3 \uparrow 7.0
S3DIS	Oracle	84.6	84.2	–	–	64.9	66.0
	Source-Only	54.5	54.9	63.2	65.9	46.1	42.1
	Joint-Train	55.5 \uparrow 1.0	56.1 \uparrow 1.2	65.4 \uparrow 2.2	66.8 \uparrow 0.9	47.0 \uparrow 0.9	42.8 \uparrow 0.7
	TENT	56.0 \uparrow 1.5	54.6 \downarrow 0.3	53.0 \downarrow 10.2	66.1 \uparrow 0.2	45.6 \downarrow 0.5	43.4 \uparrow 1.3
	DUA	59.0 \uparrow 4.5	57.6 \uparrow 2.7	67.3 \uparrow 4.1	65.5 \downarrow 0.4	46.7 \uparrow 0.6	44.1 \uparrow 2.0
	AdaContrast	58.0 \uparrow 3.5	57.5 \uparrow 2.6	65.4 \uparrow 2.2	65.6 \uparrow 0.3	46.7 \uparrow 0.6	46.4 \uparrow 4.3
	TTT-KD-O	65.0 \uparrow 10.5	64.1 \uparrow 9.2	68.8 \uparrow 5.6	68.7 \uparrow 2.8	50.1 \uparrow 4.0	49.2 \uparrow 7.1
	TTT-KD	69.9 \uparrow 14.4	68.4 \uparrow 13.5	71.7 \uparrow 8.5	71.5 \uparrow 5.6	53.2 \uparrow 7.1	50.9 \uparrow 8.8
MATT3D	Oracle	73.5	72.9	77.9	78.5	–	–
	Source-Only	49.0	45.4	59.2	58.6	55.2	53.8
	Joint-Train	52.6 \uparrow 3.6	50.6 \uparrow 5.2	59.9 \uparrow 0.7	63.7 \uparrow 5.1	56.0 \uparrow 0.8	55.4 \uparrow 1.6
	TENT	50.3 \uparrow 1.3	47.5 \uparrow 2.1	52.3 \downarrow 6.9	65.0 \uparrow 6.4	54.1 \downarrow 1.1	54.7 \uparrow 0.9
	DUA	52.7 \uparrow 3.7	50.7 \uparrow 5.3	64.5 \uparrow 5.3	63.8 \uparrow 5.2	56.0 \uparrow 0.8	54.7 \uparrow 0.9
	AdaContrast	55.2 \uparrow 6.2	53.4 \uparrow 8.0	60.8 \uparrow 1.6	69.7 \uparrow 11.1	56.0 \uparrow 0.8	54.3 \uparrow 0.5
	TTT-KD-O	59.4 \uparrow 10.4	57.6 \uparrow 12.2	64.4 \uparrow 5.2	70.9 \uparrow 12.3	57.8 \uparrow 2.6	56.2 \uparrow 2.4
	TTT-KD	64.0 \uparrow 15.0	62.6 \uparrow 17.2	66.8 \uparrow 7.6	75.4 \uparrow 16.8	58.7 \uparrow 3.5	56.5 \uparrow 2.7

Comparison to baselines. When compared to TENT, DUA, and *AdaContrast*, although these baselines can provide some adaptation, TTT-KD has a clear advantage, surpassing them by a large margin. We can see that TENT is not suited for the task of semantic segmentation, since it does not provide improvement in many of the configurations. We hypothesize this is due to the mean and standard deviation of the batch normalization layers, which TENT computes independently for each test batch. Since we are testing each scene independently, these estimates are not representative of the OOD data, leading to a degradation of performance. We can also see that DUA performs better than TENT, since it accumulates these parameters over several scenes, but still fails for some configurations. Lastly, we can see that the more complex method *AdaContrast*, performs better than both DUA and TENT but falls behind our TTT-KD. Fig. 3 presents some qualitative results of these methods.

Backbone agnostic. When we analyze the performance of our method on different backbones, we see a consistent improvement in all setups. This indicates that our method is independent of the 3D backbone used.

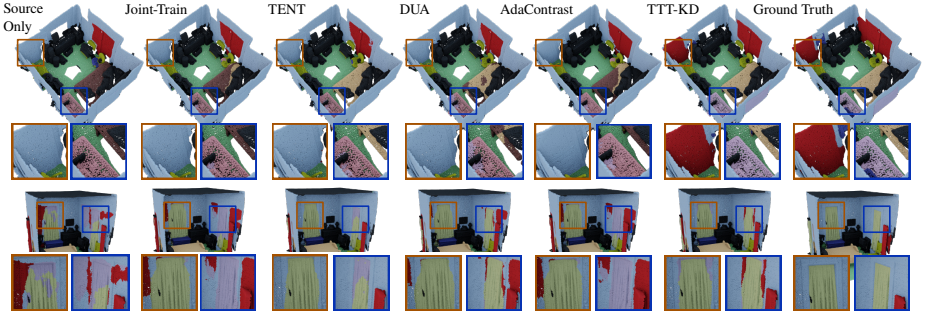


Fig. 3: Qualitative results for two different OOD tasks. The top row presents results for $\text{MATTERPORT3D} \rightarrow \text{SCANNET}$, while the bottom row presents results for $\text{SCANNET} \rightarrow \text{MATTERPORT3D}$. Although other methods are able to slightly adapt to the domain shifts, our TTT-KD algorithm provides more accurate predictions.

4.2 Outdoor 3D Semantic Segmentation

In this section, first, we briefly describe the datasets used, then the experimental setup, and lastly, we provide the results of the experiments.

Datasets. In our experiments, we use two different autonomous driving datasets of real outdoor 3D scenes, A2D2 [14] and SEMANTICKITTI [2]. While the 3D pointclouds are obtained with LiDAR scans, the images are obtained from different cameras mounted on the vehicle. Following Jaritz *et al.* [21], only the 2D images obtained from the front camera of the vehicle are used, and the 3D pointcloud is cropped by selecting only visible points from this camera. For each point in the 3D pointcloud, only 3D coordinates are used.

Experimental setup. For the task of outdoor 3D semantic segmentation, we use the same experimental setup as other UDA (xMUDA [21]) and TTA methods (MM-TTA [48]). For additional details, we refer the reader to Jaritz *et al.* [21].

Tasks. We focus on a well-established and challenging task to measure the robustness of a model to OOD data using mIoU as our metric. In this task, we train a model on the training set of the A2D2 dataset and perform TTT on the test set of the SEMANTICKITTI. Since the LiDAR scan used in the target domain is of higher resolution than the one used in the source domain, this task aims to measure the robustness of the 3D model to OOD pointcloud data.

Model. As our 3D backbone, we use the same sparse convolution architecture as previous work [21, 48]. As our foundation model, we use again DINOv2 [37].

Testing. For testing, we use the same configuration as in the indoor 3D semantic segmentation tasks. However, due to the large size of the dataset, we reduce the number of rotations to 4, and the number of TTT steps of our offline version to 25. Moreover, we reduce the learning rate of the optimizer to 0.1.

Table 2: Results for the outdoor 3D semantic segmentation tasks. Our TTT-KD algorithm significantly reduces the domain gap for OOD compared to other methods.

Method	A2D2 \rightarrow KITTI
Oracle	73.8
Source-Only	35.8
Joint-Train	41.6 \uparrow 5.8
TENT	36.6 \uparrow 0.8
xMUDA	38.0 \uparrow 2.2
MM-TTA	42.5 \uparrow 6.7
TTT-KD-O	52.0 \uparrow 16.2
TTT-KD	49.7 \uparrow 13.9

Baselines. As in the indoor datasets, we train several models: *Source-Only*, *Joint-Train*, *TTT-KD*, *TTT-KD-O*, and *Oracle*. Additionally, we compare to the 3D backbone of the 2D-3D multi-modal TTA method *MM-TTA* [48], to a TTA version of *xMUDA* [21] as in Shin *et al.* [48], and, again, to *TENT* [52].

Results. The main results of this experiment are presented on Tab. 2. In the following paragraphs, we analyze these results in detail.

Joint-Training. As in the indoor tasks, our Joint-Train strategy provides a significant improvement over the Source-Only model. Moreover, we can see that it is able to match and even surpass most of the baselines without performing any adaptation during testing, confirming that our KD secondary task acts as regularizer, improving the generalization of the model.

Out-of-distribution. When we analyze the performance of the Source-Only models when tested on OOD, we see again a significant performance drop when compared with an Oracle model trained on ID data. Our TTT-KD algorithm, on the other hand, presents a large performance increase when compared to the Source-Only. The domain gap is reduced even more by our TTT-KD-O, achieving an increase of 45% mIoU. We hypothesize that this is due to the reduced number of TTT iterations of our offline version when compared to the number of iterations used for the indoor tasks.

Comparison to baselines. When compared to commonly used baselines for TTA in outdoor 3D semantic segmentation, we can see that our TTT-KD and TTT-KD-O algorithms surpass them by a large margin. While MM-TTA is able to achieve reasonable good performance, xMUDA provides a small improvement over the Source-Only model. TENT, as in the indoor tasks, provides a marginal improvement.



Fig. 4: Ablation studies. (a) Improvement w.r.t. the number of TTT step utilized per scene. (b) mIoU of the model w.r.t. to the number of images used in our TTT-KD. (c) Comparison of DINOv2 [37] to CLIP [41] and SAM [22] as our foundation model.

4.3 Ablation Studies

In this section, we describe the ablation studies carried out to investigate the effect of different design choices on the performance of our algorithm. Unless otherwise stated, due to computational reasons, all these ablations are performed on the task of indoor 3D semantic segmentation while adapting from S3DIS \rightarrow SCANNET, with 25 TTT steps using our offline setup.

Number of TTT steps. We measure the performance of our TTT-KD algorithm in relationship to the number of TTT steps and plot the results in Fig. 4 (a). We see that the mIoU increases with the number of TTT updates, and saturates at 200 steps. However, relative improvement is reduced after 100 steps.

Number of images. Our algorithm relies on paired pointcloud and image data, which might be restrictive for some setups. Therefore, we measure the performance of our method w.r.t. the number of images used for KD. Fig. 4 (b) presents the results of this experiment. We can see that even when only a single image is used, we can achieve a boost in mIoU of 4.5. These results support the findings on the outdoor tasks, where also only one image is available for adaptation. Moreover, we can see that the improvement saturates for 5 images when the improvement obtained by including an additional image is reduced.

Foundation model. For a more generalizable TTT approach, it must work with any of the readily available *off-the-shelf* foundation models. To evaluate this, we experiment with different foundation models used for TTT-KD. In this experiment, we compare the foundation model used in our main experiments, DINOv2 [37], to a CLIP [41] model trained with 2B paired image-text data, and to a SAM [22] model trained with 11M annotated images, and provide the results in Fig. 4 (c). Although previous works [9, 37] have shown that DINOv2 provides better segmentation masks than CLIP, our TTT-KD is also able to provide considerable performance gains while using CLIP in our pipeline. Moreover, TTT-KD is able to obtain similar results when the foundation model is trained with ground truth image segmentation masks, such as the SAM model.

5 Limitations

Despite the number of benefits of our TTT-KD, it is not totally exempt from limitations. Similar to other TTT methods, the main limitation is the additional computation required for TTT in comparison to simply evaluating a network with frozen weights. Our *standard* TTT-KD requires processing each image with a foundation model and then performing several optimization steps for each scene. Still, this could be drastically reduced with our online version, which only optimizes the network weights for a single step, as other TTA methods, and shows considerable improvements even surpassing the offline version for some datasets. Another limitation is that our algorithm relies on the robustness of the foundation model to OOD data. From the experiments presented in the paper, and additional experiments provided in the appendix, we concluded that DINOv2 [37] is robust to domain shifts. However, we acknowledge that there might be some cases where the foundation model used does not present such robustness. In such cases, existing TTT or TTA approaches for 2D images could be used to adapt the foundation model to this new domain.

6 Conclusions

Our TTT-KD is the first test-time training method proposed for the task of 3D semantic segmentation, which proposes to use knowledge distillation from foundation models as a self-supervised auxiliary objective to adapt the network weights individually for each test sample as it is encountered. Our experiments show that TTT-KD can be used with any off-the-shelf foundation model and multiple different 3D backbones. Furthermore, our method provides impressive performance gains while adapting to both in-distribution and out-of-distribution test samples when evaluated on multiple different benchmarks.

References

1. Armeni, I., Sax, S., Zamir, A.R., Savarese, S.: Joint 2d-3d-semantic data for indoor scene understanding (2017)
2. Behley, J., Garbade, M., Milioto, A., Quenzel, J., Behnke, S., Stachniss, C., Gall, J.: SemanticKITTI: A Dataset for Semantic Scene Understanding of LiDAR Sequences. In: Proc. of the IEEE/CVF International Conf. on Computer Vision (ICCV) (2019)
3. Boudiaf, M., Mueller, R., Ben Ayed, I., Bertinetto, L.: Parameter-free online test-time adaptation. In: Proceedings of the IEEE/CVF Conference on Computer Vision and Pattern Recognition. pp. 8344–8353 (2022)
4. Cao, H., Xu, Y., Yang, J., Yin, P., Yuan, S., Xie, L.: Mopa: Multi-modal prior aided domain adaptation for 3d semantic segmentation (2023)
5. Chang, A., Dai, A., Funkhouser, T., Halber, M., Niessner, M., Savva, M., Song, S., Zeng, A., Zhang, Y.: Matterport3D: Learning from RGB-D data in indoor environments. International Conference on 3D Vision (3DV) (2017)
6. Chen, D., Wang, D., Darrell, T., Ebrahimi, S.: Contrastive test-time adaptation. In: Proceedings of the IEEE/CVF conference on computer vision and pattern recognition (2022)
7. Choy, C., Gwak, J.Y., Savarese, S.: 4d spatio-temporal convnets: Minkowski convolutional neural networks. In: Proceedings of the IEEE Conference on Computer Vision and Pattern Recognition (2019)
8. Dai, A., Chang, A.X., Savva, M., Halber, M., Funkhouser, T., Nießner, M.: Scannet: Richly-annotated 3d reconstructions of indoor scenes. Proc. CVPR (2017)
9. Darcet, T., Oquab, M., Mairal, J., Bojanowski, P.: Vision transformers need registers (2023)
10. Döbler, M., Marsden, R.A., Yang, B.: Robust mean teacher for continual and gradual test-time adaptation. In: Proceedings of the IEEE/CVF Conference on Computer Vision and Pattern Recognition. pp. 7704–7714 (2023)
11. Fruhwirth-Reisinger, C., Opitz, M., Possegger, H., Bischof, H.: FAST3D: Flow-Aware Self-Training for 3D Object Detectors. In: Proc. BMVC (2021)
12. Gandelsman, Y., Sun, Y., Chen, X., Efros, A.: Test-time training with masked autoencoders. Advances in Neural Information Processing Systems **35**, 29374–29385 (2022)
13. Ganin, Y., Ustinova, E., Ajakan, H., Germain, P., Larochelle, H., Laviolette, F., Marchand, M., Lempitsky, V.: Domain-Adversarial Training of Neural Networks. JMLR **17**(59), 1–35 (2016)
14. Geyer, J., Kassahun, Y., Mahmudi, M., Ricou, X., Durgesh, R., Chung, A.S., Hauswald, L., Pham, V.H., Mühlegg, M., Dorn, S., Fernandez, T., Jänicke, M., Mirashi, S., Savani, C., Sturm, M., Vorobiov, O., Oelker, M., Garreis, S., Schubert, P.: A2D2: audi autonomous driving dataset (2020), <http://www.a2d2.audi/>
15. Gidaris, S., Singh, P., Komodakis, N.: Unsupervised representation learning by predicting image rotations. arXiv preprint arXiv:1803.07728 (2018)
16. He, K., Chen, X., Xie, S., Li, Y., Dollár, P., Girshick, R.: Masked autoencoders are scalable vision learners. In: Proceedings of the IEEE/CVF conference on computer vision and pattern recognition. pp. 16000–16009 (2022)
17. Hendrycks, D., Dietterich, T.: Benchmarking neural network robustness to common corruptions and perturbations. Proceedings of the International Conference on Learning Representations (2019)
18. Hermosilla, P.: Point neighborhood embeddings (2023)

19. Ioffe, S., Szegedy, C.: Batch Normalization: Accelerating Deep Network Training by Reducing Internal Covariate Shift. In: Proc. ICML (2015)
20. Iwasawa, Y., Matsuo, Y.: Test-time classifier adjustment module for model-agnostic domain generalization. *Advances in Neural Information Processing Systems* **34**, 2427–2440 (2021)
21. Jaritz, M., Vu, T.H., de Charette, R., Wirbel, E., Pérez, P.: xMUDA: Cross-modal unsupervised domain adaptation for 3D semantic segmentation. In: Proc. CVPR (2020)
22. Kirillov, A., Mintun, E., Ravi, N., Mao, H., Rolland, C., Gustafson, L., Xiao, T., Whitehead, S., Berg, A.C., Lo, W.Y., Dollár, P., Girshick, R.: Segment anything. [arXiv:2304.02643](https://arxiv.org/abs/2304.02643) (2023)
23. Lehner, A., Gasperini, S., Marcos-Ramiro, A., Schmidt, M., Mahani, M.A.N., Navab, N., Busam, B., Tombari, F.: 3d-vfield: Adversarial augmentation of point clouds for domain generalization in 3d object detection. In: Proc. CVPR (2022)
24. Liang, H., Fan, H., Fan, Z., Wang, Y., Chen, T., Cheng, Y., Wang, Z.: Point cloud domain adaptation via masked local 3d structure prediction. In: Proc. ECCV. Springer (2022)
25. Liang, J., Hu, D., Feng, J.: Do we really need to access the source data? source hypothesis transfer for unsupervised domain adaptation. In: International conference on machine learning. pp. 6028–6039. PMLR (2020)
26. Lim, H., Kim, B., Choo, J., Choi, S.: Ttn: A domain-shift aware batch normalization in test-time adaptation. [arXiv preprint arXiv:2302.05155](https://arxiv.org/abs/2302.05155) (2023)
27. Lin, W., Mirza, M.J., Kozinski, M., Possegger, H., Kuehne, H., Bischof, H.: Video Test-Time Adaptation for Action Recognition. In: Proc. CVPR (2023)
28. Loshchilov, I., Hutter, F.: Decoupled weight decay regularization. In: Proc. ICLR (2019)
29. Luo, Z., Cai, Z., Zhou, C., Zhang, G., Zhao, H., Yi, S., Lu, S., Li, H., Zhang, S., Liu, Z.: Unsupervised Domain Adaptive 3D Detection with Multi-Level Consistency. In: Proc. CVPR (2021)
30. Malić, D., Fruhwirth-Reisinger, C., Possegger, H., Bischof, H.: Sailor: Scaling anchors via insights into latent object representation. In: Proc. WACV (2023)
31. Mirza, M.J., Shin, I., Lin, W., Schriebl, A., Sun, K., Choe, J., Kozinski, M., Possegger, H., Kweon, I.S., Yoon, K.J., Bischof, H.: Mate: Masked autoencoders are online 3d test-time learners. *Proc. ICCV* (2023)
32. Mirza, M.J., Micorek, J., Possegger, H., Bischof, H.: The Norm Must Go On: Dynamic Unsupervised Domain Adaptation by Normalization. In: Proc. CVPR (2022)
33. Mirza, M.J., Soneira, P.J., Lin, W., Kozinski, M., Possegger, H., Bischof, H.: ActMAD: Activation Matching to Align Distributions for Test-Time Training. In: Proc. CVPR (2023)
34. Nekrasov, A., Schult, J., Litany, O., Leibe, B., Engelmann, F.: Mix3D: Out-of-Context Data Augmentation for 3D Scenes. In: International Conference on 3D Vision (3DV) (2021)
35. Niu, S., Wu, J., Zhang, Y., Chen, Y., Zheng, S., Zhao, P., Tan, M.: Efficient Test-Time Model Adaptation without Forgetting. In: Proc. ICML (2022)
36. Niu, S., Wu, J., Zhang, Y., Wen, Z., Chen, Y., Zhao, P., Tan, M.: Towards stable test-time adaptation in dynamic wild world. In: International Conference on Learning Representations (2023)
37. Oquab, M., Darcet, T., Moutakanni, T., Vo, H., Szafraniec, M., Khalidov, V., Fernandez, P., Haziza, D., Massa, F., El-Nouby, A., et al.: Dinov2: Learning robust visual features without supervision. [arXiv preprint arXiv:2304.07193](https://arxiv.org/abs/2304.07193) (2023)

38. Pang, Y., Wang, W., Tay, F.E., Liu, W., Tian, Y., Yuan, L.: Masked autoencoders for point cloud self-supervised learning. In: European conference on computer vision. pp. 604–621. Springer (2022)
39. Peng, D., Lei, Y., Li, W., Zhang, P., Guo, Y.: Sparse-to-dense feature matching: Intra and inter domain cross-modal learning in domain adaptation for 3d semantic segmentation. In: Proc. ICCV (2021)
40. Qin, C., You, H., Wang, L., Kuo, C.C.J., Fu, Y.: PointDAN: A Multi-Scale 3D Domain Adaption Network for Point Cloud Representation. In: NeurIPS (2019)
41. Radford, A., Kim, J.W., Hallacy, C., Ramesh, A., Goh, G., Agarwal, S., Sastry, G., Askell, A., Mishkin, P., Clark, J., et al.: Learning transferable visual models from natural language supervision. In: International conference on machine learning (ICML) (2021)
42. Saltori, C., Galasso, F., Fiameni, G., Sebe, N., Poiesi, F., Ricci, E.: Compositional semantic mix for domain adaptation in point cloud segmentation. IEEE TPAMI (2023)
43. Saltori, C., Galasso, F., Fiameni, G., Sebe, N., Ricci, E., Poiesi, F.: Cosmix: Compositional semantic mix for domain adaptation in 3d lidar segmentation. In: Proc. ECCV (2022)
44. Saltori, C., Lathuilière, S., Sebe, N., Ricci, E., Galasso, F.: Sf-uda3d: Source-free unsupervised domain adaptation for lidar-based 3d object detection. In: Proc. i3dv (2020)
45. Shaban, A., Lee, J., Jung, S., Meng, X., Boots, B.: Lidar-uda: Self-ensembling through time for unsupervised lidar domain adaptation. In: Proc. ICCV (2023)
46. Shannon, C.E.: A mathematical theory of communication. The Bell system technical journal **27**(3), 379–423 (1948)
47. Shen, Y., Yang, Y., Yan, M., Wang, H., Zheng, Y., Guibas, L.J.: Domain Adaptation on Point Clouds via Geometry-Aware Implicits. In: Proc. CVPR (2022)
48. Shin, I., Tsai, Y.H., Zhuang, B., Schuler, S., Liu, B., Garg, S., Kweon, I.S., Yoon, K.J.: Mm-tta: Multi-modal test-time adaptation for 3d semantic segmentation. In: Proc. CVPR (2022)
49. Smith, L.N., Topin, N.: Super-convergence: Very fast training of residual networks using large learning rates (2017)
50. Sun, Y., Wang, X., Liu, Z., Miller, J., Efros, A., Hardt, M.: Test-time training with self-supervision for generalization under distribution shifts. In: International conference on machine learning. pp. 9229–9248. PMLR (2020)
51. Thomas, H., Qi, C.R., Deschaud, J.E., Marcotegui, B., Goulette, F., Guibas, L.J.: Kpconv: Flexible and deformable convolution for point clouds. Proceedings of the IEEE International Conference on Computer Vision (ICCV) (2019)
52. Wang, D., Shelhamer, E., Liu, S., Olshausen, B., Darrell, T.: Tent: Fully Test-time Adaptation by Entropy Minimization. In: Proc. ICLR (2020)
53. Wang, P.S.: Octformer: Octree-based transformers for 3d point clouds. ACM Transactions on Graphics (SIGGRAPH) (2023)
54. Wang, Q., Fink, O., Van Gool, L., Dai, D.: Continual test-time domain adaptation. In: Proceedings of the IEEE/CVF Conference on Computer Vision and Pattern Recognition. pp. 7201–7211 (2022)
55. Wang, Y., Chen, X., You, Y., Li, L.E., Hariharan, B., Campbell, M., Weinberger, K.Q., Chao, W.L.: Train in Germany, Test in The USA: Making 3D Object Detectors Generalize. In: Proc. CVPR (2020)
56. Wu, X., Tian, Z., Wen, X., Peng, B., Liu, X., Yu, K., Zhao, H.: Towards large-scale 3d representation learning with multi-dataset point prompt training (2023)

57. Wu, X., Jiang, L., Wang, P.S., Liu, Z., Liu, X., Qiao, Y., Ouyang, W., He, T., Zhao, H.: Point transformer v3: Simpler, faster, stronger. In: Proceedings of 28th IEEE Conference on Computer Vision and Pattern Recognition (2024)
58. Wu, X., Lao, Y., Jiang, L., Liu, X., Zhao, H.: Point transformer v2: Grouped vector attention and partition-based pooling. In: Advances in Neural Information Processing Systems (NeurIPS) (2022)
59. Wu, X., Tian, Z., Wen, X., Peng, B., Liu, X., Yu, K., Zhao, H.: Towards large-scale 3d representation learning with multi-dataset point prompt training. In: Proceedings of 28th IEEE Conference on Computer Vision and Pattern Recognition (2024)
60. Xing, B., Ying, X., Wang, R., Yang, J., Chen, T.: Cross-modal contrastive learning for domain adaptation in 3d semantic segmentation. In: Proc. AAAI (2023)
61. Yang, J., Shi, S., Wang, Z., Li, H., Qi, X.: ST3D: Self-training for Unsupervised Domain Adaptation on 3D Object Detection. In: Proc. CVPR (2021)
62. Yang, Y.Q., Guo, Y.X., Xiong, J.Y., Liu, Y., Pan, H., Wang, P.S., Tong, X., Guo, B.: Swin3d: A pretrained transformer backbone for 3d indoor scene understanding (2023)
63. Yi, L., Gong, B., Funkhouser, T.: Complete & label: A domain adaptation approach to semantic segmentation of lidar point clouds. In: Proc. CVPR (2021)
64. Zhang, M., Levine, S., Finn, C.: Memo: Test time robustness via adaptation and augmentation. *Advances in Neural Information Processing Systems* **35**, 38629–38642 (2022)
65. Zhao, H., Jiang, L., Jia, J., Torr, P.H., Koltun, V.: Point transformer. In: Proceedings of the IEEE International Conference on Computer Vision (ICCV) (2021)
66. Zhu, H., Yang, H., Wu, X., Huang, D., Zhang, S., He, X., He, T., Zhao, H., Shen, C., Qiao, Y., Ouyang, W.: PonderV2: Pave the way for 3d foundation model with a universal pre-training paradigm. arXiv preprint arXiv:2310.08586 (2023)

A Additional Experiments

A.1 SCANNET Benchmark

Since our TTT-KD provides a clear improvement on ID data, we compare our strategy to SOTA models on the SCANNET benchmark for 3D semantic segmentation. For this experiment, we decrease the resolution of the sub-sampling step to 2cm and keep the same data augmentation techniques as in our main experiments. Tab. 3 presents the result of this experiment. We can see that our model trained jointly with the self-supervised task provides a competitive performance, obtaining competitive validation accuracy over the supervised methods, only surpassed by the recent Point transformer v3 [57], but falling behind methods using pre-training strategies or additional data. However, when we perform TTT with our TTT-KD algorithm, we can see that it outperforms most of the existing methods on the validation set, only surpassed by the recent Point transformer v3 [57] trained with additional data, while achieving competitive performance on the test set. Please note that historically TTT methods have been proposed to adapt to OOD data only [12, 31, 50], however, our TTT-KD also shows impressive performance gains while adapting to ID data.

Table 3: Results on the test and validation sets of SCANNET. *Italic* indicates a pre-training strategy or additional data was used.

Method	Res.	Val.	Test
MinkowskiNet [7]	2cm	72.2	73.6
Point Transf. V2 [58]	2cm	75.4	75.2
PNE [18]	2cm	74.9	75.5
OctFormer [53]	1cm	75.7	76.6
Point Transf. V3 [57]	2cm	77.5	77.9
+ <i>PointPrompt</i> [59]	2cm	78.6	79.4
<i>PointPrompt</i> [59]	2cm	76.4	76.6
<i>Swin3D</i> [62]	2cm	77.5	77.9
<i>PonderV2</i> [66]	2cm	77.0	<u>78.5</u>
Joint-Train	2cm	75.7	–
TTT-KD		<u>77.6</u>	77.3

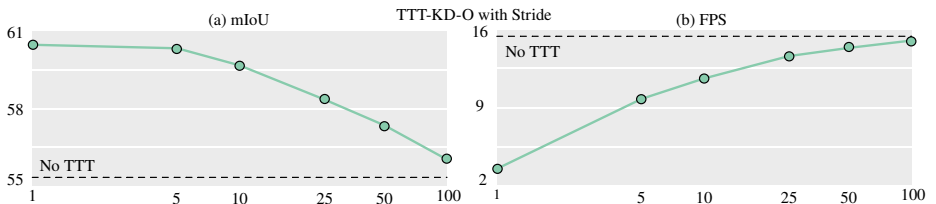


Fig. 5: Results obtained when updating the model’s parameters using our TTT-KD-O algorithm with stride s , *i.e.* only performing a TTT step every s predictions. Results show that even for large stride values our algorithm produces significant improvements while maintaining low computational cost.

A.2 Computational Cost

TTT-KD is computationally very inexpensive. All our experiments are performed on a single NVIDIA A6000 GPU, requiring 2 Gb memory and, on average,

177 ms for each TTT step in the SCANNET dataset, plus 210 ms for each image processed by the foundation model, DINOv2 ViT-L. However, if speed is a concern for some applications, we can reduce the frequency of parameter updates in our online TTT setup. Fig. 5 (a) shows, for the S3DIS \rightarrow SCANNET setup with a single image per scene, the mIoU for a different number of predictions in between each parameter update, *i.e.* a stride of 5 indicates that the parameters of the model are updated every 5 scene predictions. We can see that even if our TTT-KD-Ois sparsely applied, this still leads to a significant improvement. Moreover, Fig. 5 (b) shows the predictions per second of our method for different values of stride. We can see that, even when we apply our TTT step every 5 predictions, we can perform almost 10 predictions per second.

Additionally, since the main cost of our algorithm is the image processing with the foundation model, we could use a smaller model, such as the distilled ViT-S version of DINOv2, reducing the time from 210 ms per image to 25 ms.

A.3 Robustness of Foundation Model

One of the underlying goals of our TTT-KDis to exploit the world model inherently learned by foundation models during their large-scale pre-training and avoid fine-tuning to save computation overhead during TTT. Furthermore, DINOv2 reports strong robustness to distribution shifts, *e.g.* on ImageNet-C (IN-C) benchmark [17]. To verify this in our setup, we perturb the images with the distribution shifts proposed in the IN-C benchmark and provide the final adaptation results while adapting from S3DIS \rightarrow SCANNET in Tab. 4. We observe no performance drop by adding these corruptions. This might be because we down-sample the images by $4\times$ before feeding them to DINOv2, which alleviates the effect of distortions provoked by these perturbations.

Table 4: TTT-KD results with distribution shifted images.

<i>Source-Only</i>	ImageNet-C Corruptions				
	Clean	Shot	Blur	Bright	Jpeg
55.5	66.6	66.6	66.7	66.6	66.4

A.4 Additional Qualitative Results

Fig. 6 provides additional qualitative results.

B Datasets

B.1 Indoor 3D Semantic Segmentation

SCANNET [8]. This dataset is composed of 1,513 real 3D scans of different rooms, for which each point in the scan is classified among 20 different classes.

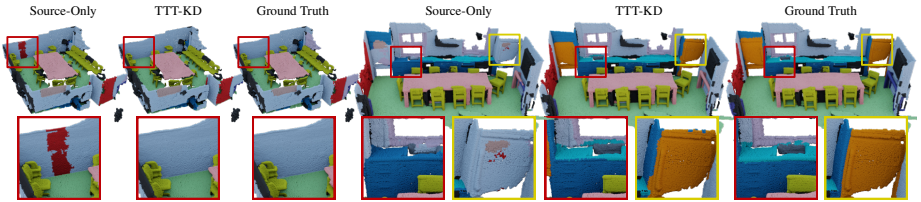


Fig. 6: Additional qualitative results of the Mink [7] network trained and tested on the SCANNET dataset. We can see that even if training and testing data are from the same distribution, our TTT-KD algorithm also improves the predictions of the model.

Moreover, for each scan, a set of images used for the 3D reconstruction is provided. The dataset is divided into two splits, 1,201 rooms for training and 312 rooms for validation. Moreover, data samples from an additional 100 rooms are provided as a test set for benchmarking where ground truth labels are not available. In our experiments, we train the models on the train set and report performance on the validation set.

S3DIS [1]. This dataset provides dense pointclouds of 271 different rooms from 6 large-scale areas. Each point in the dataset is classified among 13 different classes. The dataset also provides the 2D images used for the 3D reconstruction. Following previous works [51,65], we use data collected in areas 1, 2, 3, 4, and 6 for training and data collected in area 5 for testing.

MATTERPORT3D [5]. Matterport3D provides pointclouds from 90 building-scale scenes, each composed of multiple regions or areas, and a set of images used for the 3D reconstruction. Each point within the dataset is classified among 21 classes. We follow the official splits and use 61 scenes for training, 11 for validation, and 18 for testing. We report the performance of the models on the test split.

Data augmentations. Although it is common practice to use specific data augmentations for each data set, this might lead to a bigger generalization gap when evaluating on OOD datasets. Therefore, for a fair baseline, we use a fixed set of data augmentations for all the data sets. We use random mirror of the X, Y axes, random rotations around the up vector, random scaling, elastic distortion, jitter of point coordinates, random crop, random translation, random adjustments of brightness and contrast of the point’s colors, and RGB shift. Moreover, we subsample the scene using a voxel size of 4 cm. Lastly, we mix two scenes [34] with a probability equal to 0.5.

Semantic labels. Tbl. 5 presents the list of classes per each dataset. We can see that SCANNET and MATTERPORT3D share almost all classes with the exception of *ceilling*. However, with S3DIS the number of shared classes is only 8 with SCANNET and 9 with MATTERPORT3D .

Table 5: List of all semantic labels used on our experiments and their presence in each individual dataset.

	Bathtub	Beam	Bed	Board	Bookshelf	Cabinet	Ceiling	Chair	Clutter	Column	Counter	Curtain	Desk	Door	Floor	Otherfurniture	Picture	Refrigerator	Shower curtain	Sink	Sofa	Table	Toilet	Wall	Window
S3DIS	✓		✓	✓	✓	✓	✓	✓	✓	✓					✓	✓					✓	✓		✓	✓
SCANNET	✓		✓		✓	✓		✓			✓	✓	✓	✓	✓	✓	✓	✓	✓	✓	✓	✓	✓	✓	✓
MATT3D	✓		✓		✓	✓	✓	✓			✓	✓	✓	✓	✓	✓	✓	✓	✓	✓	✓	✓	✓	✓	✓

B.2 Outdoor 3D Semantic Segmentation

A2D2 [14]. This dataset contains multiple outdoor driving scenes of paired point clouds and images. The point clouds are obtained from three overlapping low-resolution LiDAR scans with 16 layers each that generate a rather sparse point cloud. Following the experimental setup of xMUDA [21], we only use the points that are projected on the front camera of the vehicle. For training, we use the standard split used in xMUDA, resulting in more than 27 K scenes.

SEMANTICKITTI [2]. Similar to A2D2, this dataset also contains multiple outdoor driving scenes of paired point clouds and images. The point cloud in this dataset were obtained with a single high-resolution LiDAR scan with 64 layers. Again, we follow the experimental setup of xMUDA [21], and only use the points that are projected on the front camera of the vehicle. For testing on this dataset, we use the split used in xMUDA, resulting in more than 4 K scenes.

Semantic labels. As in xMUDA [21], we select 10 shared semantic labels between the two datasets, A2D2 and SEMANTICKITTI : car, truck, bike, person, road, parking, sidewalk, building, nature, and other-objects. For more details on class mapping, we refer the reader to xMUDA [21].

C Training Details

C.1 Indoor 3D Semantic Segmentation

Training. We use AdamW [28] as our optimizer with a maximum learning rate of 0.005 and a OneCycleLR learning rate scheduler [49] with an initial division factor of 10, and a final factor of 1000. To prevent overfitting, we use a weight decay value of 0.0001 and label smoothing for the segmentation task with a value of 0.2.

Test-Time Training. For TTT, we use SGD without momentum and a learning rate equal to 1.0. We optimize 100 steps for each scene before performing the final prediction.

Number of images. For SCANNET , we used the images provided in the 25K subset, where images from the RGB-D video sequence are taken at intervals of 100, generating 16 images per scene on average. For MATTERPORT3D and S3DIS we select the available images for each scene from the provided 2D data. If more than 50 images for each scene are available, we select randomly 50.

Number of samples for KD loss. Since the knowledge distillation loss requires large amounts of GPU memory due to the large feature dimensions of the embeddings, we randomly sample 2048 points per scene during training. During testing, since we work with only one scene at a time, we increase this number of samples to 16,384 samples.

C.2 Outdoor 3D Semantic Segmentation

For the outdoor 3D semantic segmentation task, we use the same training as setup as xMUDA [21]. However, due to the large feature dimensions of the image foundation models, for the knowledge distillation loss, we use the same number of samples as in the indoor 3D semantic segmentation tasks.

D TTT-KD Algorithm

In Alg. 1 we present the detailed TTT-KDalgorithm, consisting of the joint-training, the TTT, and inference phases.

Algorithm 1: TTT-KDalgorithm.

Input: Training data $\mathcal{S} = \{(\mathcal{X}, \mathcal{F}, \mathcal{Y}, \mathcal{I}, \mathcal{U})\}$
 Test sample $(\mathcal{X}', \mathcal{F}', \mathcal{I}', \mathcal{U}')$
 3D Backbone (ψ_{3D})
 2D Foundation Model (ϕ_{2D})
 Projectors ($\rho_{\mathcal{Y}}, \rho_{2D}$)

Result: Prediction (\mathcal{Y}')

begin

```

# Joint-Training
for numEpochs do
   $(\mathcal{X}, \mathcal{F}, \mathcal{Y}, \mathcal{I}, \mathcal{U}) = \text{sampleBatch}(\mathcal{S})$ 
   $F^{3D} = \psi_{3D}(\mathcal{X}, \mathcal{F})$ 
   $\hat{\mathcal{Y}} = \rho_{\mathcal{Y}}(F^{3D})$ 
   $\hat{F}^{2D} = \rho_{2D}(F^{3D})$ 
   $F^{2D} = \phi_{2D}(\mathcal{I})$ 
   $\mathcal{L} = \mathcal{L}_{\mathcal{Y}}(\hat{\mathcal{Y}}, \mathcal{Y}) + \mathcal{L}_{2D}(\hat{F}^{2D}, F^{2D}, \mathcal{U})$ 
   $\mathcal{L}.\text{backward}()$ 
   $\text{optimizer}.\text{step}()$ 
 $\mathcal{Y}' = 0$ 
for numRotations do
   $\hat{\mathcal{X}}' = \text{Rotate}(\mathcal{X}')$ 
  # Test-Time Training
  for numTTTSteps do
     $\hat{F}^{2D} = \rho_{2D}(\psi_{3D}(\hat{\mathcal{X}}', \mathcal{F}'))$ 
     $F^{2D} = \phi_{2D}(\mathcal{I}')$ 
     $\mathcal{L} = \mathcal{L}_{2D}(\hat{F}^{2D}, F^{2D}, \mathcal{U}')$ 
     $\mathcal{L}.\text{backward}()$ 
     $\text{optimizer}.\text{step}()$ 
  # Inference
   $\mathcal{Y}' += \rho_{\mathcal{Y}}(\psi_{3D}(\mathcal{X}', \mathcal{F}'))$ 

```
